A minimal flow unit of the logarithmic layer in the absence of near-wall eddies and large scales

By H. J. Bae† AND A. Lozano-Durán

1. Motivation and objectives

In the vicinity of walls, turbulent flows are found to be highly organized, consisting of streamwise rolls and low- and high-speed streaks (Klebanoff *et al.* 1962; Kline *et al.* 1967; Smith & Metzler 1983; Blackwelder & Eckelmann 1979; Johansson *et al.* 1987) that are involved in a quasi-periodic regeneration cycle (Robinson 1991; Panton 2001; Adrian 2007; Smits *et al.* 2011; Jiménez 2018). Important progress regarding the study of this regeneration cycle was made using the "minimal flow unit" approach, which indicated that buffer layer streaks can self-sustain even when motions at larger scales are inhibited and that their existence, therefore, relies on an autonomous process (Jiménez & Moin 1991). The observation that the buffer and viscous layers of wall-bounded flows can be simulated in periodic boxes of minimal dimensions has been useful in understanding wall turbulence since it enables the study of individual flow features in isolation from their mutual interactions.

The minimal simulation boxes for the buffer layer of turbulent channels have been extended to the logarithmic (log) and outer regions, where they contain a segment of streamwise velocity streak, and a vortex cluster (or streamwise roll) (Flores & Jiménez 2010). Contrary to the minimal flow unit for the buffer layer, intermediate flow units allow for self-sustained motions of scales smaller than the flow unit extension. While the minimal flow unit for log layers demonstrates that a similar but more disorganized scenario occurs for the log layer (Flores & Jiménez 2010; Lozano-Durán *et al.* 2012; Lozano-Durán & Jiménez 2014; Hwang & Bengana 2016; Cossu & Hwang 2017; Lozano-Durán *et al.* 2019), and it is known that destroying the dynamics of the buffer layer has essentially no influence over the statistics of the outer flow (Townsend 1976; Perry & Abell 1977; Jiménez 2004; Bakken *et al.* 2005; Flores & Jiménez 2006; Flores *et al.* 2007; Mizuno & Jiménez 2013; Chung *et al.* 2014; Lozano-Durán & Bae 2019*a*), the larger boxes isolate more complicated, fully multiscale structures that reach from the wall farther into the core flow, making it harder to identify individual flow features to be studied as in the buffer-layer case.

Large-eddy simulations (LES) with the static Smagorinsky model (Smagorinsky 1963) have been used in an attempt to isolate larger structures in the log region from the near-wall cycle and from the background smaller scales in turbulent channel (Hwang & Cossu 2010, 2011; Hwang & Bengana 2016) and plane Couette (Rawat *et al.* 2015) flows. This approach, termed overdamped LES, is based on the idea that by increasing the Smagorinsky parameter, an increasing range of small-scale structures is accounted for by the subgrid-scale model, whereas large structures are resolved by the LES grid (Cossu & Hwang 2017). However, recent findings suggest that overdamped LES represent

† Graduate Aerospace Laboratories, California Institute of Technology, Pasadena, CA

enlarged/modified near-wall streaks from an effective reduction of the Reynolds number rather than structures isolated from the original near-wall cycle (Feldmann & Avila 2018).

Recently, Lozano-Durán & Bae (2019*a*) performed simulations of a turbulent channel flow, where the no-slip wall is replaced by a Robin boundary condition for the three velocity components. The results showed that the outer-layer one-point statistics and spectra of this modified channel agree quantitatively with those of its no-slip counterpart while suppressing the formation of near-wall small scales. Moreover, the Robin boundary condition imposes a new length scale on the eddies in the near-wall region such that the size of the active energy-containing eddies at the boundary (wall) is scaled in outer units rather than in wall units.

Our goal in this brief is to present and discuss a flow configuration that isolates a portion of the log layer by limiting the formation of larger outer-layer structures while suppressing the formation of the near-wall eddies. We achieve this by applying the Robin boundary condition in a minimal flow unit for a log region. This method, in addition to isolating the log-layer eddies, can utilize the scale separation in the entirety of the domain such that LES can be performed without the restrictive grid-resolution requirements near the wall for no-slip walls. We perform direct numerical simulation (DNS) and LES of the proposed setup to demonstrate that the log-layer structures can be isolated using one-point statistics and energy spectra.

The brief is organized as follows. In Section 2, we introduce the numerical experiment of the minimal flow unit of the log layer using the Robin boundary condition. We provide one-point statistics and spectra of this channel flow in comparison with traditional channels in Section 3 and instantaneous velocity profiles in Section 4. We summarize our results in Section 5.

2. Numerical experiment

A DNS of a channel flow between two parallel walls is performed by discretizing the incompressible Navier-Stokes equations with a staggered, second-order accurate, central finite-difference method in space (Orlandi 2000), and an explicit third-order accurate Runge-Kutta method for time advancement (Wray 1990). The system of equations is solved via an operator-splitting approach (Chorin 1968). The streamwise, wall-normal and spanwise directions are denoted by x_i, $i = 1, 2, 3$, respectively, and the corresponding velocity components are given by u_i with $i = 1, 2, 3$. Periodic boundary conditions are imposed in the streamwise and spanwise directions, and the boundary conditions in x_2 are given by the Robin boundary condition of the form

$$u_i|_w = l_s \left. \frac{\partial u_i}{\partial n} \right|_w, \; i = 1, 2, 3, \tag{2.1}$$

where l_s is the slip length, the subscript w refers to quantities evaluated at the boundary, and n is the x_2-boundary-normal direction (or wall-normal direction, in analogy to the wall-bounded case). The LES utilizes the same numerical methods and boundary conditions as the DNS with the addition of the subgrid-scale (SGS) model. For the SGS model, we use the anisotropic minimum dissipation model (Rozema *et al.* 2015). The code has been validated in previous studies of turbulent channel flows using no-slip (Bae *et al.* 2018, 2019) and Robin boundary conditions (Lozano-Durán & Bae 2019*a*).

The friction Reynolds number of the simulation is $Re_\tau = u_\tau \delta / \nu \approx 2003$, where δ is the channel half-height, ν is the kinematic viscosity, and u_τ is the friction velocity at the wall computed from the total stress. This number gives a conservative estimate of the log

region between $140 \leq x_2^+ \leq 300$ (Marusic *et al.* 2013), where wall units denoted by the superscript + are defined in terms of ν and u_τ. The streamwise, wall-normal, and spanwise domain sizes of the simulation are $L_1/\delta \approx 1.57$, $L_2/\delta = 2$, and $L_3/\delta \approx 0.79$, respectively. This domain size corresponds to a minimal box simulation for the log layer and is sufficient to isolate the relevant dynamical structures involved in the bursting process (Flores & Jiménez 2010). Moreover, the choice of the domain size is such that the wall-normal distance below which flow exhibits healthy turbulence, $l_d \approx L_3/3 \approx 0.25\delta$ (Flores & Jiménez 2010), is above the upper bound of the log layer. For the DNS, the domain is discretized using $N_1 = N_3 = 512$ points in the streamwise and spanwise directions and $N_2 = 901$ points in the wall-normal direction. The grid spacings in the streamwise and spanwise directions are uniform with $\Delta_1^+ \approx 6.2$ and $\Delta_3^+ \approx 3.1$; non-uniform meshes are used in the wall-normal direction, with the grid stretched toward the wall according to a hyperbolic tangent distribution with $\min(\Delta_2^+) \approx 0.56$ and $\max(\Delta_2^+) \approx 9.6$. For the LES, the domain is discretized using $N_1 = 256$ and $N_3 = 64$ points in the streamwise and spanwise directions, and the grid spacings in the streamwise and spanwise directions are $\Delta_1/\delta \approx 0.006$ and $\Delta_3/\delta \approx 0.012$ such that the grid captures 90% of the turbulent kinetic energy at $x_2/\delta = 0.15$, which is necessary to accurately capture the coherent structures present in the flow (Lozano-Durán & Bae 2019*b*). The grid in the wall-normal direction is coarsened by a factor of 9. Note that the grid resolution for the LES scales in outer units and, thus, can be kept constant with increasing Reynolds number as long as the slip length is held constant. However, for a direct comparison with DNS data, we use $Re_\tau \approx 2003$ to validate the performance of LES for this setup. We set the slip length $l_s/\delta = 0.05$, such that the adaptation length (Lozano-Durán & Bae 2019*a*), i.e., the vertical distance from the boundary above which the flow recovers to the nominal no-slip flow statistics, $l_a \approx l_s$, is below the lower bound of the log layer for this Reynolds number.

We compare our cases, labeled R-M2000 for the DNS and R-M2000-LES for the LES, with the no-slip DNS data of a channel with domain size $L_1 \times L_2 \times L_3 = 8\pi\delta \times 2\delta \times 3\pi\delta$ from Hoyas & Jiménez (2006), which we label as NS-L2000.

3. One-point statistics and spectra

Figure 1 shows the mean streamwise velocity profile $\langle u_1 \rangle$ for the present cases in comparison with NS-L2000. Here, $\langle \cdot \rangle$ indicates averaged values in homogeneous directions and time, and $(\cdot)'$ indicates fluctuating quantities with respect to the mean. In Figure 1(b), the mean profiles for the present cases are vertically by 8.5 wall units such that the mean profile of the R-L2000 case matches that of the NS-L2000 case at $x_2/\delta = 0.2$. The reduction in the total mass flux is due to the Robin boundary condition. However, this shift can be modified trivially by either adding a constant uniform velocity to the right-hand side of the Robin boundary condition or by a Galilean transformation of the velocity field. We observe that the shape of the mean velocity profile remains roughly identical to NS-L2000 in the log region for both cases. The deviation below $x_2 \approx l_a$ is due to the disruption of the viscous scaling from imposing the Robin boundary condition (Lozano-Durán & Bae 2019*a*); the overprediction of the mean velocity profile from $x_2 \approx l_d$ to the centerline is due to the restrictive domain size, as discussed in Flores & Jiménez (2010). In the log region, here defined as $140\nu/u_\tau \leq x_2 \leq 0.2\delta$, the mean velocity profile follows the same log profile as that of the no-slip large-domain counterpart.

The characteristic length scales of the current DNS case are plotted in Figure 2(a).

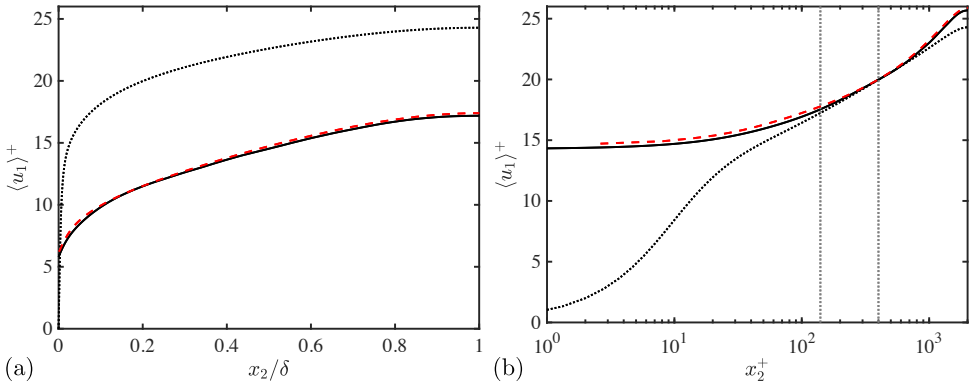

FIGURE 1. Mean streamwise velocity profiles as a function of x_2 in (a) linear scale and (b) log scale for R-M2000 (solid), R-M2000-LES (dashed) and NS-L2000 (dotted). In (b), the velocity profile of R-M2000 and R-M2000-LES is vertically shifted by 8.5 wall units such that the velocity at $x_2/\delta = 0.2$ for the DNS coincides with the velocity of NS-L2000. Dotted straight lines indicate $x_2^+ = 140$ and $x_2/\delta = 0.2$.

The small scales are represented by the Kolmogorov length scale $\eta = (\nu^3/\langle\varepsilon\rangle)^{1/4}$, and the large scales are represented by the shear length scale $L_s = u_\tau/(d\langle u_1\rangle/dx_2)$. The two length scales of R-M2000 deviate from that of NS-L2000 close to the wall. It has been shown that the large scales remain roughly constant in the Robin-bounded cases regardless of the Reynolds number and that the energy-containing eddies at the wall scale in outer units rather than in the classic viscous units (Lozano-Durán & Bae 2019*a*). This is a consequence of the interruption of the classic near-wall cycle, thus showing that the Robin boundary condition is successful at suppressing the formation of the viscous- and buffer-layer dynamics. The suppression of the viscous layer is also an indication that the LES of the present case does not need the restrictive grid-resolution requirements in the near-wall region for no-slip walls. In the outer region, the shear length scale is smaller for R-M2000 than that for NS-L2000. This finding is consistent with the smaller simulation box, as larger scales are artificially removed due to the restricted domain size. However, the length scales of both cases are in good agreement in the log region, consistent with the results presented for the mean velocity profile.

Figure 2(b,c,d) shows the streamwise, wall-normal and spanwise root-mean-square (r.m.s.) velocity fluctuations for R-M2000, R-M2000-LES, and NS-L2000. The R-M2000 and R-M2000-LES show good agreement for all r.m.s. fluctuations in the log region, with a slight underprediction of the streamwise component. This mismatch can be attributed to the filtering of the small scales that are modeled in the LES. Compared to NS-L2000, the streamwise velocity fluctuations lack the near-wall peak at $x_2^+ \approx 15$ as expected from a Robin-bounded case. Moreover, the profiles for the wall-normal velocity intensities are almost the same in the three cases for $x_2 < l_d$, as anticipated from the minimal box size. The streamwise and spanwise fluctuations are lower in the R-M2000 and R-M2000-LES cases than in the full channel due to the lack of large scales, and they are known to be progressively damped as the box size is reduced (Flores & Jiménez 2010). This is because the minimal boxes are large enough to contain a substantial fraction of the wall-normal energy, but only a small part of the streamwise streaks in the log layer.

This phenomenon can be observed in the two-dimensional premultiplied energy spectra at $x_2/\delta = 0.15$ shown in Figure 3. The dotted line, indicating the box size of R-M2000

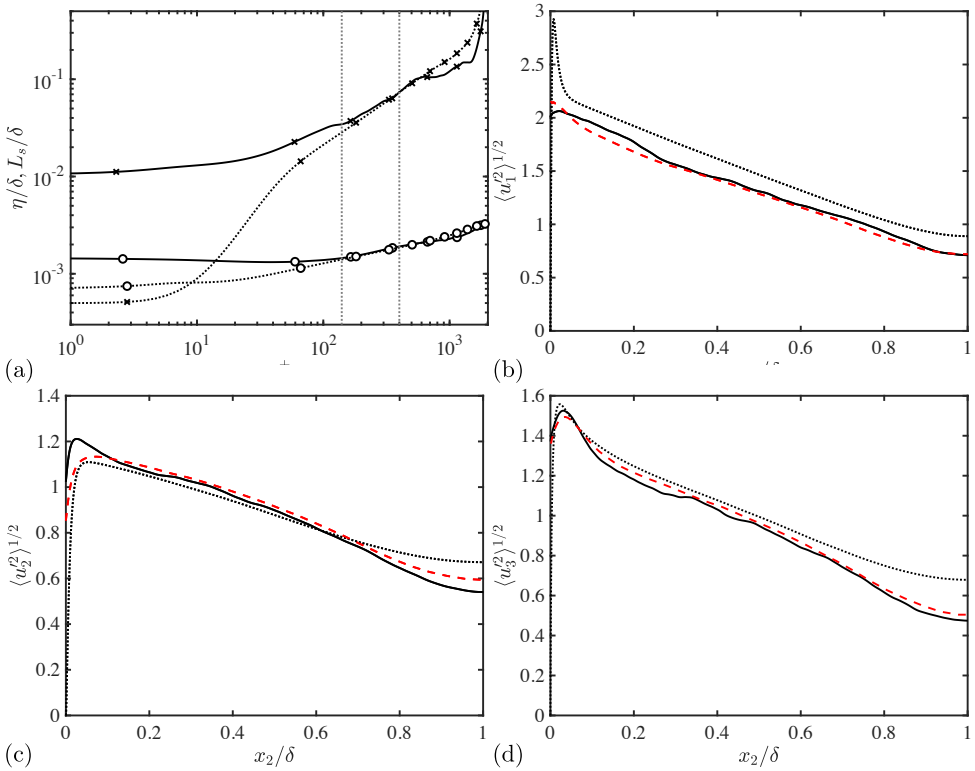

FIGURE 2. (a) Kolmogorov (circles) and shear (crosses) length scales as a function of x_2 for R-M2000 (solid) and NS-L2000 (dotted). Dotted lines indicate $x_2^+ = 140$ and $x_2/\delta = 0.2$. (b) Streamwise, (c) wall-normal, and (d) spanwise r.m.s. velocity fluctuations for R-M2000 (solid), R-M2000-LES (dashed), and NS-L2000 (dotted).

case, resolves only a small fraction of the total energy for the streamwise and spanwise (not shown) velocity component, whereas it encapsulates most of the energy in the wall-normal direction. Nonetheless, the energy spectra of the current DNS case agree well with the NS-L2000 case up to the smallest nonzero numerical wavenumbers resolved, as is expected from previous observations (Del Alamo *et al.* 2004; Flores & Jiménez 2010; Lozano-Durán & Bae 2019*a*). The LES case matches the spectra for the large scales but is damped for the small scales, as expected. Note that the spectra are more damped in the streamwise direction compared to the spanwise direction, indicating that the streamwise direction must be better resolved to capture more of the energetic scales. This is contrary to common LES practice, where the resolution in the streamwise component is typically several times that of the spanwise component.

The reduction of the streamwise fluctuations in the log region of the present cases is in contrast to what is observed in overdamped LES, where the streamwise r.m.s fluctuation significantly increases in the log layer (Hwang 2015; Hwang & Bengana 2016; Feldmann & Avila 2018) for both the minimal and full domains, which is unphysical for a system where the small (and large) scales are damped. The increase in the streamwise fluctuations in overdamped LES is due to the alteration of the dynamics in such a way that the streaks

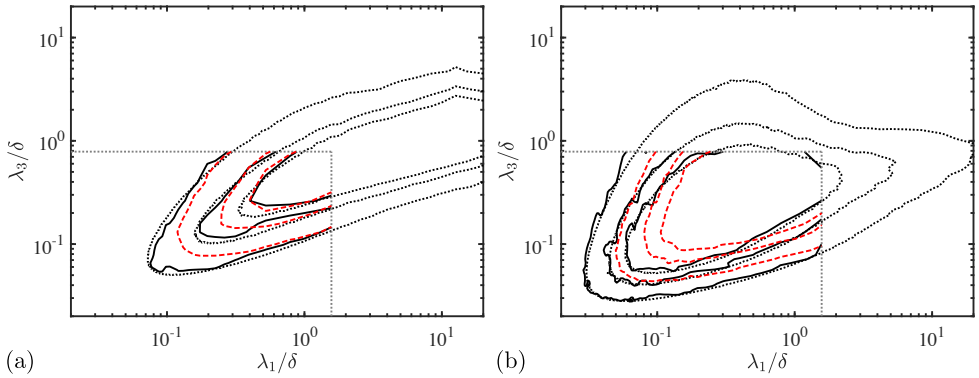

FIGURE 3. Two-dimensional premultiplied (a) streamwise and (b) wall-normal velocity spectra for R-M2000 (solid), R-M2000-LES (dashed) and NS-L2000 (dotted) at $x_2/\delta = 0.15$. Contours are 0.1, 0.3 and 0.5 of the maximum of values from NS-L2000. Straight dotted lines indicate the domain size of the minimal flow unit.

are unable to follow their natural cycle of meandering and breakup (Waleffe *et al.* 1993; Jiménez & Pinelli 1999), which is often observed in under-resolved LES (Bae *et al.* 2018).

The agreement of one-point statistics and spectra between the present cases with the larger-domain no-slip channel case suggests that the dynamics of the log layer is fairly independent of the buffer and outer layers. Moreover, the disruption of the viscous scaling in the buffer layer and the restriction of larger scales in the outer region effectively isolate healthy turbulence to the log layer, which can be simulated using LES with a grid resolution that scales in outer units.

4. Instantaneous velocity fluctuations

Figures 4(a,b) show instantaneous streamwise velocity fluctuations for R-M2000 at two different instances in time. The most notable feature is the absence of the streaky structures in the buffer layer, as expected in a no-slip wall. The lack of near-wall streaks is apparent in the comparison of instantaneous snapshots of the streamwise velocity fluctuation at $y^+ = 15$ between R-M2000 and NS-L2000, plotted in Figure 5. Moreover, the single large streak in the log layer is detached from the wall and is present in both a straight (Figure 4(a)) and meandering (Figure 4(b)) form. However, the streak does not resemble the simple continuous ribbon-like structures of streamwise velocity fluctuations observed in minimal flow units of the buffer layer or the overdamped LES of higher Reynolds numbers, the latter of which results in a stronger streamwise fluctuation compared to the unaltered turbulent channel. While the current setup allows the structures in the log region to sustain in the absence of buffer- or outer-layer dynamics, the full multiscale interaction within the log region is captured. Because of the wider range of scales involved in the log region compared to those of the buffer region, the coherent structures examined here are expected to be different from those in the buffer region.

Filtering the velocity fluctuations allows the large-scale structures to be observed without the intricate details of the small scales. Figures 4(c,d) show the Gaussian-filtered instantaneous streamwise velocity fluctuation of R-M2000,

$$\mathcal{F}(u_1') = \iint_{-\infty}^{\infty} \int_{0}^{2\delta} \frac{1}{\sqrt{2\pi}\sigma^3} \exp\left(-\frac{x_1^2 + x_2^2 + x_3^2}{2\sigma^2}\right) u_1' \, \mathrm{d}x_2 \mathrm{d}x_1 \mathrm{d}x_3, \tag{4.1}$$

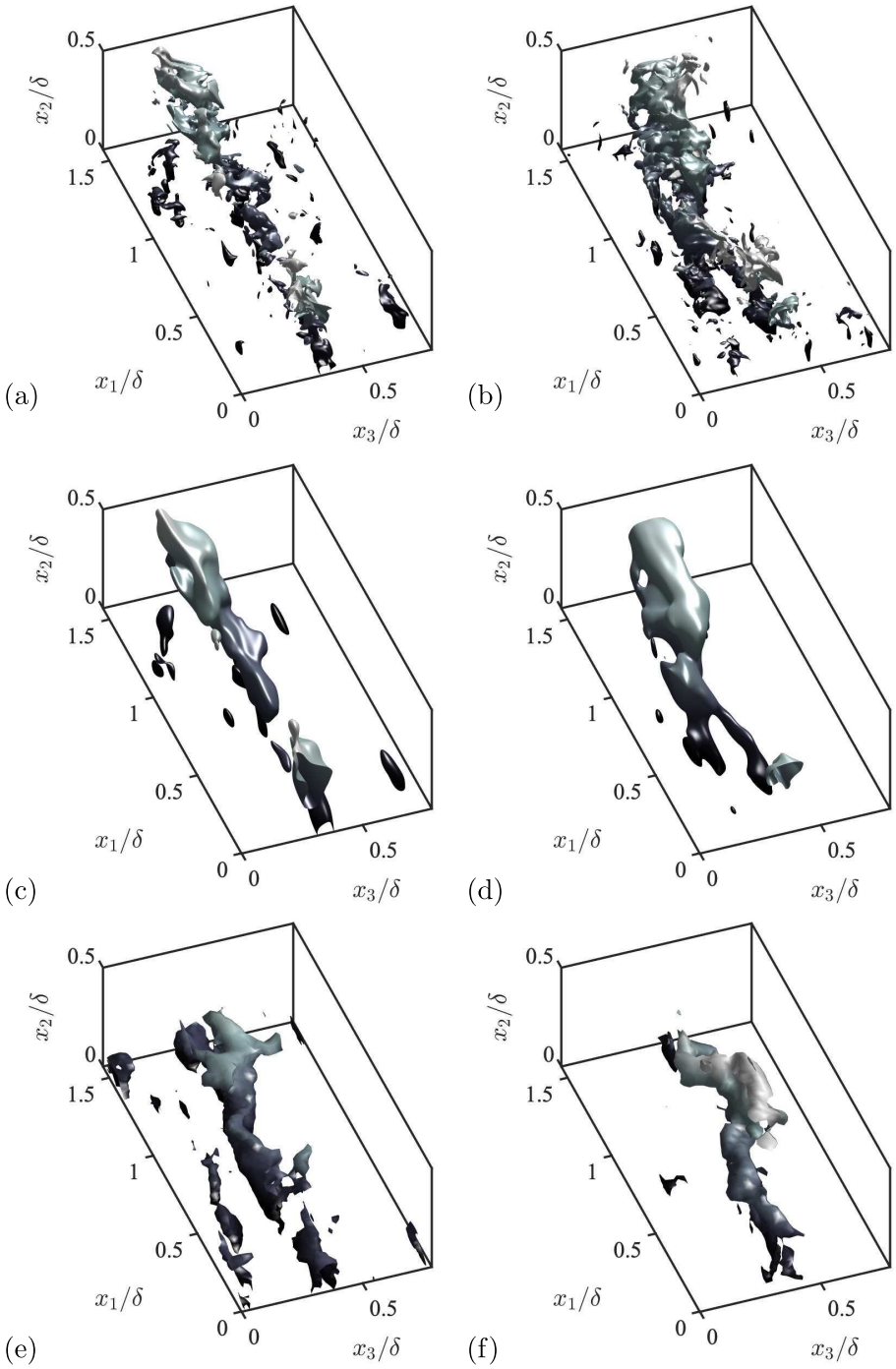

FIGURE 4. Isosurfaces of (a,b) instantaneous streamwise velocity fluctuation $u_1'^+ = -3.2$ and (c,d) filtered instantaneous streamwise velocity fluctuation $\mathcal{F}(u_1')^+ = -2.5$ at two different time instances for R-M2000. The shades indicate distance from the wall. (e,f) Isosurfaces of instantaneous streamwise velocity fluctuation $u_1'^+ = -3.2$ at two different time instances for R-M2000-LES.

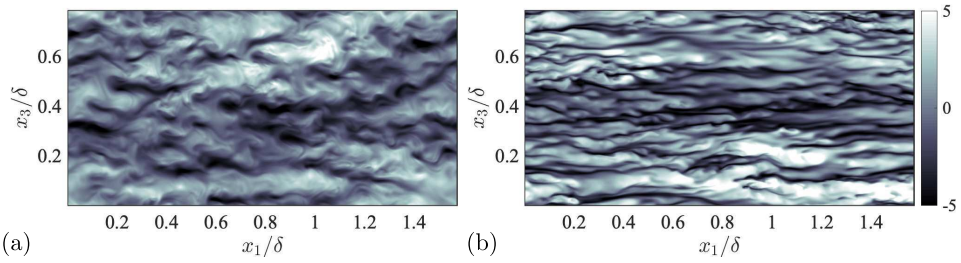

FIGURE 5. Instantaneous streamwise velocity fluctuations $u_1'^+$ at $x_2^+ = 15$ for (a) R-M2000 and (b) NS-L2000.

with the filter width $\sigma = 0.1\delta$ at the same time instances as in Figures 4(a,b). Due to the limitation imposed by the wall, the Gaussian filter acts as a one-sided filter close to the wall, progressively damping more fluctuations closer to the wall. However, the structures we are concerned with are fairly detached from the wall, and the filter choice has little impact on the resulting velocity fluctuations. The filtered velocity fluctuations show the same streamwise streak as that in Figure 4(a) but with less noise from the small scales. We also include qualitatively equivalent snapshots from the R-M2000-LES case in Figure 4(e,f). These snapshots show similar structures to those of the filtered streamwise velocity fluctuations, indicating that the LES is able to capture the dynamics of the large-scales in the log layer.

5. Summary

In this brief, we have devised a numerical experiment isolating the dynamics of the log region without the effect of the buffer layer or outer region. This is achieved by applying a Robin boundary condition at the walls to remove the viscous scaling close to the wall and thus disrupting the buffer layer dynamics, while simultaneously limiting the domain size such that the scales larger than the minimal flow unit are artificially omitted. We show that both the DNS and the LES of the current setup match the one-point statistics as well as the energy spectra of the regular channel in the log layer, with the exception of the streamwise velocity fluctuations, which are under-predicted as the large scales are purposefully removed from the simulation. Thus, the log layer dynamics can sustain on its own without energy from the buffer or outer region. In addition, the LES grid-resolution requirements of this experiment scale in outer units, potentially allowing simulations of portions of the log layer at extremely large Reynolds numbers using the same grid resolution provided in this brief. This setup will allow the study of the log region on its own without the effect of the near-wall cycle. In the future, we plan to use this numerical experiment to study the self-sustaining process of wall-bounded flows limited to the log region.

Acknowledgments

A.L.-D. acknowledges the support of NASA under grant no. NNX15AU93A and of ONR under grant no. N00014-16-S-BA10.

REFERENCES

Adrian, R. J. 2007 Hairpin vortex organization in wall turbulence. *Phys. Fluids* **19**, 041301.

Bae, H. J., Lozano-Durán, A., Bose, S. T. & Moin, P. 2018 Turbulence intensities in large-eddy simulation of wall-bounded flows. *Phys. Rev. Fluids* **3**, 014610.

Bae, H. J., Lozano-Durán, A., Bose, S. T. & Moin, P. 2019 Dynamic slip wall model for large-eddy simulation. *J. Fluid Mech.* **859**, 400–432.

Bakken, O. M., Krogstad, P.-Å., Ashrafian, A. & Andersson, H. I. 2005 Reynolds number effects in the outer layer of the turbulent flow in a channel with rough walls. *Phys. Fluids* **17**, 065101.

Blackwelder, R. F. & Eckelmann, H. 1979 Streamwise vortices associated with the bursting phenomenon. *J. Fluid Mech.* **94**, 577–594.

Chorin, A. J. 1968 Numerical solution of the Navier-Stokes equations. *Math. Comput.* **22**, 745–762.

Chung, D., Monty, J. P. & Ooi, A. 2014 An idealised assessment of Townsend's outer-layer similarity hypothesis for wall turbulence. *J. Fluid Mech.* **742**.

Cossu, C. & Hwang, Y. 2017 Self-sustaining processes at all scales in wall-bounded turbulent shear flows. *Philos. Trans. Royal Soc.* **375**, 20160088.

Del Alamo, J. C., Jiménez, J., Zandonade, P. & Moser, R. D. 2004 Scaling of the energy spectra of turbulent channels. *J. Fluid Mech.* **500**, 135–144.

Feldmann, D. & Avila, M. 2018 Overdamped large-eddy simulations of turbulent pipe flow up to $Re_\tau = 1500$. In *J. Phys. Conf. Ser.*, , vol. 1001, p. 012016. IOP Publishing.

Flores, O. & Jiménez, J. 2006 Effect of wall-boundary disturbances on turbulent channel flows. *J. Fluid Mech.* **566**, 357–376.

Flores, O. & Jiménez, J. 2010 Hierarchy of minimal flow units in the logarithmic layer. *Phys. Fluids* **22**, 071704.

Flores, O., Jiménez, J. & Del Alamo, J. C. 2007 Vorticity organization in the outer layer of turbulent channels with disturbed walls. *J. Fluid Mech.* **591**, 145–154.

Hoyas, S. & Jiménez, J. 2006 Scaling of the velocity fluctuations in turbulent channels up to $Re_\tau = 2003$. *Phys. Fluids* **18**, 011702.

Hwang, Y. 2015 Statistical structure of self-sustaining attached eddies in turbulent channel flow. *J. Fluid Mech.* **767**, 254–289.

Hwang, Y. & Bengana, Y. 2016 Self-sustaining process of minimal attached eddies in turbulent channel flow. *J. Fluid Mech.* **795**, 708–738.

Hwang, Y. & Cossu, C. 2010 Self-sustained process at large scales in turbulent channel flow. *Phys. Rev. Lett.* **105**, 044505.

Hwang, Y. & Cossu, C. 2011 Self-sustained processes in the logarithmic layer of turbulent channel flows. *Phys. Fluids* **23**, 061702.

Jiménez, J. 2004 Turbulent flows over rough walls. *Annu. Rev. Fluid Mech.* **36**, 173–196.

Jiménez, J. 2018 Coherent structures in wall-bounded turbulence. *J. Fluid Mech.* **842**.

Jiménez, J. & Moin, P. 1991 The minimal flow unit in near-wall turbulence. *J. Fluid Mech.* **225**, 213–240.

Jiménez, J. & Pinelli, A. 1999 The autonomous cycle of near-wall turbulence. *J. Fluid Mech.* **389**, 335–359.

Johansson, A. V., Her, J.-Y. & Haritonidis, J. H. 1987 On the generation of

high-amplitude wall-pressure peaks in turbulent boundary layers and spots. *J. Fluid Mech.* **175**, 119–142.

Klebanoff, P. S., Tidstrom, K. D. & Sargent, L. M. 1962 The three-dimensional nature of boundary-layer instability. *J. Fluid Mech.* **12**, 1–34.

Kline, S. J., Reynolds, W. C., Schraub, F. A. & Runstadler, P. W. 1967 The structure of turbulent boundary layers. *J. Fluid Mech.* **30**, 741–773.

Lozano-Durán, A. & Bae, H. J. 2019*a* Characteristic scales of Townsends wall-attached eddies. *J. Fluid Mech.* **868**, 698–725.

Lozano-Durán, A. & Bae, H. J. 2019*b* Error scaling of large-eddy simulation in the outer region of wall-bounded turbulence. *J. Comput. Phys.* **392**, 532–555.

Lozano-Durán, A., Bae, H. J. & Encinar, M. P. 2019 Causality of energy-containing eddies in wall turbulence. *J. Fluid Mech.* .

Lozano-Durán, A., Flores, O. & Jiménez, J. 2012 The three-dimensional structure of momentum transfer in turbulent channels. *J. Fluid Mech.* **694**, 100–130.

Lozano-Durán, A. & Jiménez, J. 2014 Time-resolved evolution of coherent structures in turbulent channels: characterization of eddies and cascades. *J. Fluid Mech.* **759**, 432–471.

Marusic, I., Monty, J. P., Hultmark, M. & Smits, A. J. 2013 On the logarithmic region in wall turbulence. *J. Fluid Mech.* **716**.

Mizuno, Y. & Jiménez, J. 2013 Wall turbulence without walls. *J. Fluid Mech.* **723**, 429–455.

Orlandi, P. 2000 *Fluid Flow Phenomena: A Numerical Toolkit*, *Fluid Flow Phenomena: A Numerical Toolkit*, vol. 55. Springer.

Panton, R. L. 2001 Overview of the self-sustaining mechanisms of wall turbulence. *Prog. Aerosp. Sci.* **37**, 341–383.

Perry, A. E. & Abell, C. J. 1977 Asymptotic similarity of turbulence structures in smooth-and rough-walled pipes. *J. Fluid Mech.* **79**, 785–799.

Rawat, S., Cossu, C., Hwang, Y. & Rincon, F. 2015 On the self-sustained nature of large-scale motions in turbulent Couette flow. *J. Fluid Mech.* **782**, 515–540.

Robinson, S. K. 1991 Coherent motions in the turbulent boundary layer. *Ann. Rev. Fluid Mech.* **23**, 601–639.

Rozema, W., Bae, H. J., Moin, P. & Verstappen, R. 2015 Minimum-dissipation models for large-eddy simulation. *Phys. Fluids* **27**, 085107.

Smagorinsky, J. 1963 General circulation experiments with the primitive equations: I. The basic experiment. *Mon. Weather Rev.* **91**, 99–164.

Smith, C. R. & Metzler, S. P. 1983 The characteristics of low-speed streaks in the near-wall region of a turbulent boundary layer. *J. Fluid Mech.* **129**, 27–54.

Smits, A. J., McKeon, B. J. & Marusic, I. 2011 High–Reynolds number wall turbulence. *Ann. Rev. Fluid Mech.* **43**.

Townsend, A. A. 1976 *The structure of turbulent shear flow*. Cambridge university press.

Waleffe, F., Kim, J. & Hamilton, J. M. 1993 On the origin of streaks in turbulent shear flows. In *Turbulent Shear Flows 8*, pp. 37–49. Springer.

Wray, A. A. 1990 Minimal-storage time advancement schemes for spectral methods. *Tech. Rep.*. NASA Ames Research Center.